Available online at www.sciencedirect.com
SCIENCE DIRECT®
Solar Energy 79 (2005) 122–130
SOLAR ENERGY
www.elsevier.com/locate/solener

# Potential of quarterwave interference stacks for colored thermal solar collectors

A. Schüler [a,*], C. Roecker [a], J. Boudaden [b], P. Oelhafen [b], J.-L. Scartezzini [a]

[a] *Laboratoire d'Energie Solaire et de Physique du Bâtiment LESO-PB, Ecole Polytechnique Fédérale de Lausanne EPFL, Bâtiment LE, 1015 Lausanne, Switzerland*
[b] *Institut für Physik der Universität Basel, Klingelbergstr. 82, CH-4056 Basel, Switzerland*

Received 16 April 2004; received in revised form 14 October 2004; accepted 1 December 2004
Available online 25 February 2005
Communicated by: Associate Editor Sanjay Vijayaraghavan

**Abstract**

The architectural integration of thermal solar collectors into buildings is often limited by their black color and the visibility of tubes and corrugations of the absorber sheets. A certain freedom in color choice would be desirable, but the colored appearance should not cause excessive energy losses. Multilayered interference filters on the collector glazing can produce a colored reflection, hiding the corrugated metal sheet, while transmitting the non-reflected radiation entirely to the absorber. We investigate the potential of quarterwave stacks by simulation of their optical behavior, yielding the visible reflectance $R_{VIS}$, the solar transmittance $T_{sol}$, a figure of merit $M = R_{VIS}/R_{sol}$, and the CIE color coordinates. The necessary number of individual layers in the multilayer stack as well as the choice of refractive indices and thus of thin film materials are discussed. Finally, examples for realistic multilayer designs are proposed.


*Keywords:* Colored solar collectors; Coatings for thermal collectors; Collector glazing; Dielectric thin films; Interference filters

## 1. Introduction

Architectural integration of solar energy systems into buildings has become a widely recognized issue (Hestnes, 1999; Roecker et al., 1995; Hagemann, 2002; Scartezzini and Courret, 2002), which regards techniques ranging from photovoltaics and daylighting to thermal solar energy conversion. Thermal solar collectors, typically equipped with black, optical selective absorber sheets, in general exhibit good energy conversion efficiencies. However, the black color, and sometimes the visibility of tubes and corrugations of the metal sheets, limit the architectural integration into buildings. A recent opinion poll (Weiss and Stadler, 2001) showed that 85% of architects would prefer other colors besides black, even if a lower efficiency was the price to pay. Various attempts have been made to overcome this drawback. One option is to color the absorber sheets. Optical selective absorber coatings are usually deposited by processes such as magnetron sputtering (Graf et al., 1997; Schüler et al., 2000, 2001), vacuum evaporation (Lazarov et al., 1995), electrochemical processes (Tabor, 1955), sol–gel technology (Kaluza et al., 2001), or as selective paint (thickness-sensitive or thickness-insensitive) (Orel et al., 1986; Crnjak Orel

* Corresponding author. Tel.: +41 21 693 4544.
*E-mail address:* andreas.schueler@epfl.ch (A. Schüler).

0038-092X/$ - see front matter © 2005 Elsevier Ltd. All rights reserved.
doi:10.1016/j.solener.2004.12.008

et al., 1990; Crnjak Orel and Gunde, 2001; Orel et al., 2003). Niklasson and Granqvist described the pioneering work in this area within a comprehensive overview (Niklasson and Granqvist, 1983). The above mentioned coating processes are usually optimized for high solar absorption, typically yielding black or dark blue surfaces. However, modifying the process parameters can result in a colored appearance. By varying layer thicknesses, for example, sputtered absorber coatings can be colored in a large variety of shades. Also selective paints can be prepared to exhibit other colors, such as for example blue, green, and brownish red. Following this approach, the absorber surface combines the functions of optical selectivity (high solar absorption/low thermal emission) and colored reflection. Tripanagnostopoulos reports a different solution: his group used non-selective colored paints as absorber coatings for glazed and unglazed collectors, and compensated the energy losses by additional booster reflectors (Tripanagnostopoulos et al., 2000). An alternative option to solve the problem is to establish a colored reflection not from the absorber but from the collector glazing. Interference colors of dielectric thin films are ideally suited for this purpose. Coloring the bulk glass by colors of absorption would mainly affect the transmission color, and in addition to that, useful energy would be lost. Extensive literature exists about multilayer interference stacks for various optics and laser applications (see Macleod, 2001 and references therein), but to the knowledge of the authors, only few deals with its application as energy-efficient coloration of solar thermal collectors. For multilayered thin films on solar collector glazing several constraints exist. The possible range of the refractive indices of the individual layers depends on the availability of durable thin film materials. In addition, the maximum number of layers is limited. In contrast to applications such as laser interference filters, solar applications typically employ large surfaces to be coated at low price, which implies that production costs limit the number of individual layers building up the multilayer stack. In many cases, quarterwave interference stacks are designed as broadband reflection filters, consisting of numerous individual layers and exhibiting a nearly perfect reflection over a broad frequency range (Macleod, 2001). This paper will focus on quarterwave stacks reflecting a rather narrow frequency band. We will investigate whether it is possible to achieve reasonable results with only a few individual layers, and study the proper choice of refractive indices.

## 2. Theoretical potential of colored glazed or unglazed solar collectors

The solar reflectance $R_{sol}$, corresponding to the solar energy losses, can be defined based on the hemispherical reflectance $R(\lambda)$:

$$R_{sol} = \frac{\int R(\lambda) \cdot I_{sol}(\lambda)\,d\lambda}{\int I_{sol}(\lambda)\,d\lambda}, \quad (1)$$

where the solar spectrum AM1.5 global is used as $I_{sol}(\lambda)$ (for reference spectra see Hulstrom et al., 1985; ASTM, 2004).

The visible reflectance $R_{VIS}$ is a measure for the brightness of a surface as it appears to the human eye under certain illumination conditions. A white surface or a perfect mirror exhibits 100% visible reflectance, colored or grey surfaces less. The determination of the visible reflectance $R_{VIS}$ is based on the photopic luminous efficiency function $V(\lambda)$ and depends on the choice of the illuminant $I_{ILL}(\lambda)$:

$$R_{VIS} = \frac{\int R(\lambda) \cdot I_{ILL}(\lambda) \cdot V(\lambda)\,d\lambda}{\int I_{ILL}(\lambda) \cdot V(\lambda)\,d\lambda}, \quad (2)$$

where $R(\lambda)$ is the simulated or measured hemispherical reflectance of the sample.

The International Commission on Illumination (CIE, Commission Internationale d'Eclairage) described how to quantify colors (CIE, 1986). All existing colors can be represented in a plane and mapped by Cartesian coordinates, as shown in the CIE Chromaticity Diagrams. The quantification is based on the 1931 CIE Color Matching Functions $x(\lambda)$, $y(\lambda)$, and $z(\lambda)$, which reflect the color sensitivity of the human eye. These functions depend to some extent on the width of the observation field (we will use the functions for an opening angle of 2°).

The human eye perceives only a small part of the solar spectrum; large spectral regions in ultraviolet and in infrared are invisible. This is illustrated by Fig. 1,

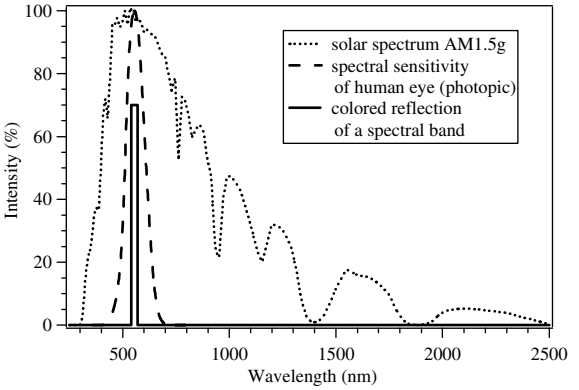


Fig. 1. Solar spectrum AM1.5g, the photopic luminous efficiency function $V(\lambda)$, and an idealized, boxcar-shaped spectrum of a colored reflection. For the evaluation of the general potential of colored solar collectors, we consider the case of the reflection of a narrow spectral band centered at the wavelength $\lambda_0$, with the width $w$ tending towards zero. The solar spectrum and the photopic luminous efficiency function are normalized with their maximum at 100%.

which shows the solar spectrum AM1.5 and the photopic luminous efficiency function $V(\lambda)$. In theory, a colored solar collector might just reflect a narrow frequency band in the visible range, thus giving rise to a colored appearance. The non-reflected part of the solar spectrum should be completely converted to thermal energy. A corresponding idealized reflectance spectrum is added to Fig. 1. The narrow spectral band of the width $w$ centered at the wavelength $\lambda_0$ can be described as follows:

$$R(\lambda) = C \quad \text{for } \lambda_0 - 1/2w \leqslant \lambda \leqslant \lambda_0 + 1/2w, \quad \text{and}$$
$$R(\lambda) = 0 \quad \text{else.} \tag{3}$$

Using this reflectance spectrum, let us compute the visible reflectance $R_{\mathrm{VIS}}$ under illumination $I_{\mathrm{ILL}}(\lambda)$. We consider the limit for $w$ small ($w \to 0$):

$$R_{\mathrm{VIS}} = \frac{\int_{\lambda_0-1/2w}^{\lambda_0+1/2w} C \cdot I_{\mathrm{ILL}}(\lambda) \cdot V(\lambda)\,\mathrm{d}\lambda}{\int I_{\mathrm{ILL}}(\lambda) \cdot V(\lambda)\,\mathrm{d}\lambda} = \frac{w \cdot C \cdot I_{\mathrm{ILL}}(\lambda_0) \cdot V(\lambda_0)}{\int I_{\mathrm{ILL}}(\lambda) \cdot V(\lambda)\,\mathrm{d}\lambda}. \tag{4}$$

The solar reflectance $R_{\mathrm{sol}}$ is computed in a similar way ($w$ small):

$$R_{\mathrm{sol}} = \frac{\int_{\lambda_0-1/2w}^{\lambda_0+1/2w} C \cdot I_{\mathrm{sol}}(\lambda)\,\mathrm{d}\lambda}{\int I_{\mathrm{sol}}(\lambda)\,\mathrm{d}\lambda} = \frac{w \cdot C \cdot I_{\mathrm{sol}}(\lambda_0)}{\int I_{\mathrm{sol}}(\lambda)\,\mathrm{d}\lambda}. \tag{5}$$

At this point it is useful to introduce a figure of merit. In a previous publication (Schüler et al., 2004) we defined the ratio of the visible reflectance $R_{\mathrm{VIS}}$ under daylight illumination $D_{65}$ and the solar reflectance $R_{\mathrm{sol}}$ (based on the solar spectrum AM1.5 global) as figure of merit $M$:

$$M = (R_{\mathrm{VIS}} \text{ under daylight illumination } D_{65}) \,/ (R_{\mathrm{sol}} \text{ for AM1.5 global}). \tag{6}$$

$M$ is large in the case of high visible reflectance or low solar energy losses $R_{\mathrm{sol}}$. This number describes the energy efficiency of the visual perception (“brightness per energy cost”). Following this definition, we obtain for the narrow spectral band centered at the wavelength $\lambda_0$ in the limit where the width $w$ goes to zero:

$$M(\lambda_0) = \frac{R_{\mathrm{VIS}}(\lambda_0)}{R_{\mathrm{sol}}(\lambda_0)} = \frac{D_{65}(\lambda_0) \cdot V(\lambda_0)}{I_{\mathrm{sol}}(\lambda_0)} \cdot \frac{\int I_{\mathrm{sol}}(\lambda)\,\mathrm{d}\lambda}{\int D_{65}(\lambda) \cdot V(\lambda)\,\mathrm{d}\lambda}. \tag{7}$$

Here an important advantage of the definition used in Eq. (6) becomes apparent: Eq. (7) depends no longer on the intensity but only on the position of the narrow frequency band.

The shape of the curve for $M(\lambda_0)$, which exhibits a maximum around 550 nm (corresponding to the color of yellow green), reflects the shape of curve $V(\lambda)$. However, the normalization is important: at the maximum, an absolute value of approximately six is reached. In this ideal case, a visible reflectance of 6% costs only 1% of the solar energy. If we desired a visible reflectance of 12%, which is already considerable for a color (since 100% corresponds to white), we would have to sacrifice only 2% of the incident energy. Since all arbitrary spectra can be regarded as superpositions of narrow spectral bands, and the corresponding integrals are linear, this maximum value of six represents the principal upper limit for $M(\lambda_0)$. This fundamental upper limit applies to all colored solar collectors, glazed or unglazed, and is valid for reflectance spectra of all possible shapes.

## 3. Simulations of quarterwave stacks

As an alternative to coloring the absorber sheet of a glazed solar collector, we propose to deposit a colored coating on the inner or outer side of the collector glazing, or on both (see Fig. 2). This coating should reflect a color, but transmit the complementary spectrum. No absorption should occur in the coating. This approach has the advantage that the black absorber sheet, which might exhibit unwanted undulations of the thin metal sheet or welding traces, is then hidden by the colored reflection. Additionally, the functions of optical selectivity and colored reflection are separated, giving more freedom to coating optimization.

An optical multilayer of plane-parallel thin films on a substrate can be considered as a stratified medium. The propagation of electromagnetic waves in stratified media has been discussed by Born and Wolf (Born and Wolf, 1999). The field of optics of thin films has been reviewed by various authors (e.g. Heavens, 1955; Holland, 1956; Anders, 1965; Knittl, 1976; Macleod, 2001). Due to multiple reflections between the different interfaces, the problem of the optical behavior of a multilayered thin film stack is non-trivial. It can be treated, though, by

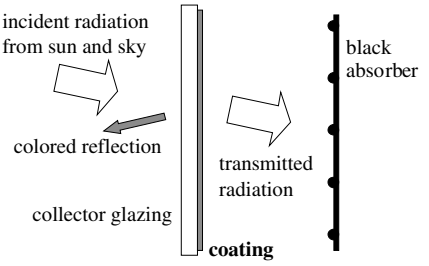


Fig. 2. Schematic drawing of a thermal solar collector, where a colored coating is applied to the collector glazing. This coating should reflect a color, thus hiding the corrugated absorber sheet, but it should transmit the complementary spectrum. No absorption should occur in the coating. Interference colors of dielectric thin films are ideally suited for this purpose. The coating can be deposited on the inner side of the collector glazing, as shown in the drawing, but also on the outer side, or on both.

the method of characteristic matrices, which defines one matrix $M_r$ per individual layer (with the layer no. $r$). The whole layer stack is then represented by the matrix product.

$$\left\{\prod_{r=1}^{q} M_r\right\} = \left\{\prod_{r=1}^{q} \begin{bmatrix} \cos\delta_r & (\mathrm{i}\sin\delta_r)/\eta_r \\ \mathrm{i}\eta_r \sin\delta_r & \cos\delta_r \end{bmatrix}\right\}, \qquad (8)$$

employing the tilted optical admittance $\eta_r$ and the phase shifts $\delta_r = 2\pi N_r d_r \cos\vartheta_r/\lambda$. Here, $N_r = n_r - \mathrm{i}k_r$ is the complex refractive index, and $\vartheta_r$ the corresponding complex angle. From this matrix product, transmission and reflectance spectra can be computed. Extended calculations are usually carried out by a computer.

In quarterwave stacks, all individual layers are of the optical film thickness $n \cdot t = \lambda_0/4$, where $\lambda_0$ is called the design wavelength. Usually layers of a high index material (H) alternate with layers of a low refractive index material (L) resulting, for example, in a stack of the form HLHLHL... The larger the difference in the refractive indices, the larger is the spectral region of high reflection. We are interested in the opposite, a narrow reflectance peak. Therefore we chose the refractive indices to be very close to each other (but not identical). Because the reflection at each interface is weak now, we need a considerable number of layers. Making the somewhat arbitrary choice of forty, our model has the form glass//(LH)^20//air. For a graphical representation see Fig. 3(a). With a design wavelength of 550 nm in mind, the following parameters were chosen: for the low refractive index material $n = 1.47$ and a thickness of 93.5 nm; for the high index material $n = 1.5$ and 91.7 nm; for the glass substrate $n = 1.52$; and for the air $n = 1$. Considering the reflection at one coated side of the glazing, we computed the reflectance of the system glass//coating//air for normal incidence with the aid of the methods described above. Indeed, we generated the shape of a narrow peak at the design wavelength 550 nm, with a maximum reflectance of around 30% (Fig. 3(b)). The full width at half maximum (FWHM) for this peak amounts to 21 nm. The peak emerges from a weak oscillation around the value of the uncoated glass (4%). For comparison, the photopic luminous efficiency function $V(\lambda)$ and the solar spectrum AM1.5, both normalized with their maximum at 100%, are added to the graph. The calculated reflectance curve, showing an isolated narrow peak and low reflectance in the rest of the solar spectrum, approximates satisfactorily the proposed boxcar-shaped function displayed in Fig. 1. The spectrum yields the color coordinates $x = 0.31$, $y = 0.47$ (yellowish green), and the visible reflectance $R_{\mathrm{VIS}} = 9.1\%$. Assuming that the other side of the substrate is neither anti-reflected nor differently coated, we calculated the reflectance of the total system. Taking into account the multiple reflections between the two sides of the glass of a thickness of several mm

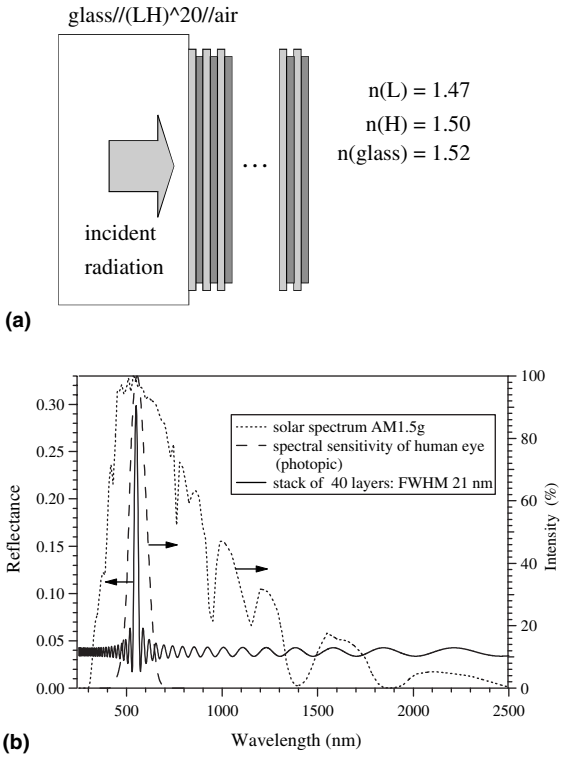


Fig. 3. (a) Schematic drawing of a quarterwave stack consisting of forty individual layers. The optical model has the structure glass//(LH)^20//air. The refractive indices amount to 1.5 and 1.47 for the high and the low index material, respectively. We simulate the reflection at the coated backside of the glass. (b) Reflectance spectrum (solid line), as computed for the optical model in (a). For comparison the solar spectrum AM1.5g and the photopic luminous efficiency function $V(\lambda)$, both normalized with their maximum at 100%, are added to the diagram.

(greater than the coherence length of sunlight), the intensities of the beams are added, and not their amplitudes. Due to the additional reflection from the uncoated surface, the resulting color turned out to be a little less saturated ($x = 0.31$, $y = 0.41$, $R_{\mathrm{VIS}} = 12.7\%$). Reflectance spectra corresponding to varying angles of incidence (0°, 20°, 40°, and 60°) have been calculated for the complete system air//glass//(LH)^20//air and are shown in Fig. 4(a). For larger angles of incidence, the peak shifts towards shorter wavelengths (obtained positions: for 0° 550 nm, for 20° 535 nm, for 40° 496 nm, and for 60° 447 nm). This blueshift is typical for interference filters and related to the phase shift $\delta_r$, which occurs in the matrix formula and is proportional to the expression $\cos\vartheta_r/\lambda$. In the calculated spectra for high angles, the background level rises, leading to less saturated colors (obtained color coordinates: for 0° $x = 0.31$, $y = 0.41$; for 20° $x = 0.29$, $y = 0.41$; for 40° $x = 0.28$, $y = 0.34$; and for 60° $x = 0.29$, $y = 0.28$). The trajectories in $x, y$

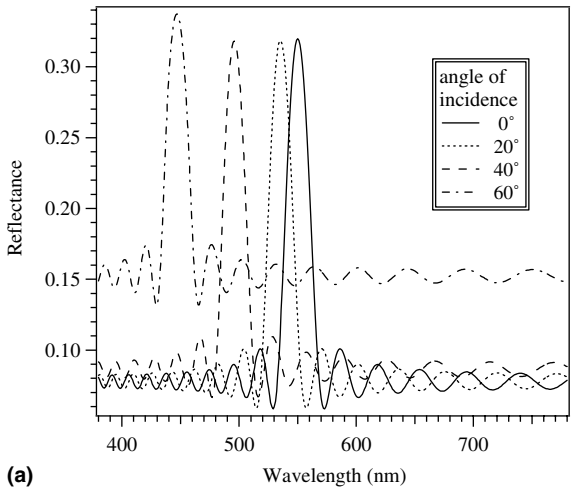


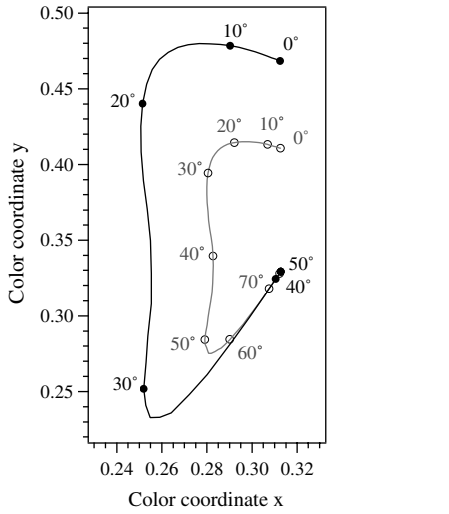


Fig. 4. (a) Angular dependence of the reflectance spectra as computed for the total system air//glass//(LH)^20//air. With a rising angle of incidence the peak shifts towards shorter wavelengths. This blueshift is related to the phase shift $\delta_r$, which occurs in the matrix formula and is proportional to the expression $\cos\vartheta_r/\lambda$. In the reflectance spectra for high angles, the background level rises, leading to less saturated colors. (b) Trajectories in $x,y$ color space for the optical models glass//(LH)^20//air (black curve, solid circles) and air//glass//(LH)^20//air (grey curve, open circles). For the latter, colors are generally less saturated and change less rapidly as a function of the angle of reflection.

color space for the optical models glass//(LH)^20//air (black curve, solid circles) and air//glass//(LH)^20//air (grey curve, open circles) are illustrated in Fig. 4(b). For the latter, colors are generally less saturated and change less rapidly as a function of the angle of reflection.

For large area production, it is always advantageous to work with the least number of individual layers. How many layers are necessary to produce a sufficiently large, isolated, and not too broad peak in reflectance? In order to attain a considerable reflection at the interfaces, we choose a larger difference between the refractive indices, employing $n(\mathrm{H}) = 1.65$ for the high index material H, and $n(\mathrm{L}) = 1.47$ for the low index material L. These values also have the advantage that they correspond roughly to silicon dioxide and aluminum oxide, respectively (Macleod, 2001; Heavens and Smith, 1957). The refractive index of the substrate (1.52) now lies between the indices of the two layer materials. From the Fresnel coefficients (see e.g. Bergmann and Schaefer, 1999) the phase jumps for the reflection at an interface can be derived. In the case of a transition from a lower refractive index to a higher refractive index, and in the absence of absorption ($n_1$ and $n_2$ real and $n_1 < n_2$, Fresnel coefficient real and negative), a phase jump of $\pi$ is found, while for the transition from a higher refractive index to a lower one no phase jump occurs (Fresnel coefficient real and positive). These relations imply the order of the layers demanding that the terminating layer should be the one with the higher index of refraction. A model with the structure glass//H(LH)^$m$//air is thus chosen, with $m = 1,2,3,\ldots$ Here again, H indicates the high index material and L the low index material. We simulate the reflection and transmission at a likewise coated side of the substrate. The resulting reflectance spectra for $m = 1,2,\ldots,7$ (3–15 individual layers) are displayed in Fig. 5. For $m = 1$ (3 layers), a relatively broad feature around the design wavelength 550 nm is formed. For five layers ($m = 2$), a pronounced reflectance peak is emerging. The corresponding spectrum is represented by the solid line. It is characterized by a maximum

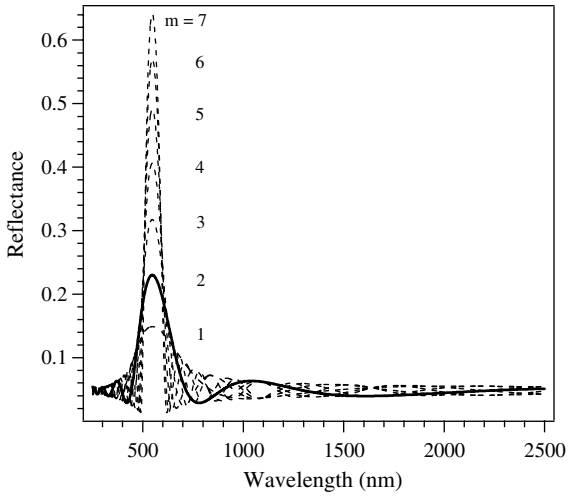


Fig. 5. Computed reflectance spectra for fewer layers. The optical model has the structure (glass//H(LH)^$m$//air), with $m = 1,2,3,\ldots$ Adding more layer pairs to the stack yields narrower and more distinct peaks.

Table 1
Color coordinates $x$ and $y$, the full width at half maximum FWHM, the value $R_{max}$ of maximum reflectance, the visible reflectance $R_{VIS}$, the solar transmission $T_{sol}$, and the figure of merit $M = R_{VIS}/R_{sol}$, as computed for the curves displayed in Fig. 5

| $m$ | $x$ | $y$ | FWHM [nm] | $R_{max}$ | $R_{VIS}$ [%] | $T_{sol}$ [%] | $M = R_{VIS}/R_{sol}$ |
|---|---|---|---|---|---|---|---|
| 1 | 0.33 | 0.38 | 234 | 0.15 | 14 | 92 | 1.8 |
| 2 | 0.35 | 0.45 | 156 | 0.23 | 20 | 91 | 2.3 |
| 3 | 0.36 | 0.50 | 124 | 0.32 | 26 | 90 | 2.6 |
| 4 | 0.35 | 0.53 | 102 | 0.41 | 31 | 90 | 3.1 |
| 5 | 0.34 | 0.54 | 90 | 0.49 | 35 | 89 | 3.1 |
| 6 | 0.33 | 0.55 | 81 | 0.57 | 38 | 89 | 3.4 |
| 7 | 0.33 | 0.56 | 76 | 0.64 | 40 | 88 | 3.4 |

reflectance of 23%, with a FWHM of 156 nm. The color of reflection is yellow-green ($x = 0.35$, $y = 0.45$), the visible reflectance considerable (20%), and the solar transmission rather high (91%). Adding more pairs of layers to the stack yields narrower and more distinct peaks leading to an increase in color saturation and visible reflectance and to a slight decrease in solar transmission. A survey of the resulting figures, the color coordinates $x$ and $y$, the full width at half maximum FWHM, the value $R_{max}$ of maximum reflectance, the visible reflectance $R_{VIS}$, the solar transmission $T_{sol}$, and the figure of merit $M = R_{VIS}/R_{sol}$ are given in Table 1. The figure of merit $M$ increases gradually from 1.8 (for 3 layers) to 3.4 (for 15 layers).

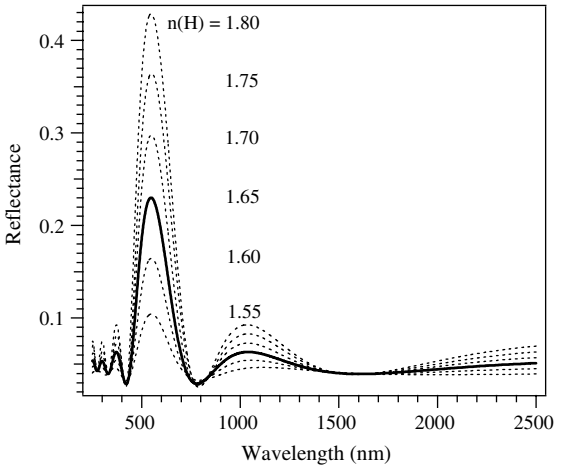


Fig. 6. Variation of the refractive index $n$(H) of the high index material, for a quarterwave stack of 5 individual layers ($m = 2$). The optical thickness $n(H) \times t(H)$ has always been kept at $\lambda/4$ ($\lambda = 550$ nm). By increasing $n$(H), substantial peak heights can be achieved. The peaks get not only higher but also moderately broader.

Let us keep the number of layers to five ($m = 2$) and vary the refractive index $n$(H) of the high index material, dimensioning the optical thickness $n(H) \times t(H)$ of the latter always to $\lambda/4$ ($\lambda = 550$ nm). Here again, only the reflection at the backside of the glass substrate is modelled. The refractive index $n$(H) has been varied from 1.55 to 1.80 in steps of 0.05. The obtained curves are depicted in Fig. 6. The spectrum for $n(H) = 1.65$ is already known from the last calculation and is again represented by the solid line. By changing the difference of the refractive indices $n(H) - n(L)$, the peak formation can easily be controlled. By increasing $n$(H), substantial peak heights can be achieved (for $n(H) = 1.80$ a maximum reflectance of 43%), yielding considerable relative luminosities (for $n(H) = 1.80$ a visible reflectance of 39%). The peaks not only get higher but also moderately broader (FWHM 180 nm at $n(H) = 1.80$ compared to e.g. 156 nm at $n(H) = 1.65$). In spite of this broadening, the figure of merit $M$ increases from 1.6 (for $n(H) = 1.55$) to 2.6 (for $n(H) = 1.8$). For $n(H) \leqslant 1.6$, the color coordinates remain nearly constant. The numerical results for the characteristic figures ($x$, $y$, FWHM, $R_{max}$, $R_{VIS}$, $T_{sol}$, $M$) are displayed in Table 2.

Table 2
Color coordinates $x$ and $y$, the full width at half maximum FWHM, the value $R_{max}$ of maximum reflectance, the visible reflectance $R_{VIS}$, the solar transmission $T_{sol}$, and the figure of merit $M = R_{VIS}/R_{sol}$, as computed for the curves displayed in Fig. 6

| $n$(H) | $x$ | $y$ | FWHM [nm] | $R_{max}$ | $R_{VIS}$ [%] | $T_{sol}$ [%] | $M = R_{VIS}/R_{sol}$ |
|---|---|---|---|---|---|---|---|
| 1.55 | 0.34 | 0.42 | 144 | 0.10 | 9 | 94 | 1.6 |
| 1.60 | 0.35 | 0.44 | 152 | 0.16 | 15 | 93 | 2.1 |
| 1.65 | 0.35 | 0.45 | 156 | 0.23 | 20 | 91 | 2.3 |
| 1.70 | 0.36 | 0.46 | 164 | 0.30 | 27 | 89 | 2.4 |
| 1.75 | 0.36 | 0.46 | 174 | 0.36 | 33 | 87 | 2.5 |
| 1.80 | 0.35 | 0.45 | 180 | 0.43 | 39 | 85 | 2.6 |

## 4. Discussion

As principal upper limit for $M$ the factor of approximately six has been found. This value indicates a large potential: in this ideal case, six percent of visible reflectance cost only one percent in solar transmission, or, even more striking, twelve percent visible reflectance cost only two percent of solar transmission. Twelve percent visible reflectance represent already a considerable value for a colored, non-white surface, while two percent reflectance losses can be regarded as moderate, compared to the reflectance losses of an uncoated glass pane (8%). In contrast to photovoltaic systems, where cell area is precious, the surface area of the thermal collectors generates only a fraction of the total system costs (the total system including pumps, boiler, stock, tubing, etc.). Therefore, for solar thermal systems, the loss of some percent in transmission can more easily be compensated with a larger receiving area. Colored glazing hiding the absorber structure would promote facade integration of solar thermal systems. Vertical facade collectors are especially advantageous for the winter season, when the sun is closer to the horizon and thermal energy is needed. Additionally, vertical facade collectors are less exposed to the sun during summertime and thus better protected against overheating. In the case of Central European latitudes, for example, the mean irradiation on vertical south-facing surfaces even exhibits a plateau during the whole time span from March to October, and decreases only moderately during wintertime, as illustrated by a recent Austrian study (Stadler, 2001). With the vertical orientation the overheating problem can thus be reduced, and the collector area can be dimensioned more generously, leading to a better match of heat offer and demand.

The general characteristics of quarterwave stacks have been illustrated by the examples above: when targeting narrow reflectance peaks, the difference in the refractive indices of the two coating materials should be sufficiently small. In order to create a considerable peak in spite of a small difference in refractive indices, the number of individual layers needs to be sufficiently high. The more layers, the higher is the peak; the closer the refractive indices, the lower and narrower is the peak. The ideal case of an isolated, narrow peak could be approximated by a stack of numerous (forty) layers, yielding a peak width of only 21 nm. Furthermore, it has been demonstrated that the quarterwave principle leads to reasonable results already for five individual layers. This is not completely out of reach for large area production. When employing refractive indices comparable to those of silicon dioxide and aluminum oxide, the resulting peaks are not too broad to yield colors of reasonable saturation.

The angular dependence of the color of reflection is related to the phase shifts $\delta_r$, and thus inherent to interference filters. One can reduce the angular color variation by combining a rough, mat outer surface or a bulk diffusing glass with the colored coating on the inner backside. The resulting angle integrated spectrum can be approximated by a weighted mean value of the spectra for the different angles. Brilliant surfaces might be interesting for modern style office buildings, while rough, mat surfaces might be an interesting alternative for residential buildings.

Aiming at a certain generality, the optical dispersion of the materials has been neglected in the given examples. At this stage of the development this approximation can be justified by the fact that in most cases the refractive indices of thin films depend on the deposition conditions and vary to some extent. Thus, in order to finally refine the coating design, it might be helpful to base the computation on measured data for the relevant process. Common thin film deposition processes are magnetron sputtering, plasma enhanced chemical vapor deposition, vacuum evaporation, or sol–gel dip coating. Transparent oxides such as silicon dioxide ($n \approx 1.47$), aluminum oxide ($n \approx 1.65$), or titanium dioxide ($n \approx 2.2$) can routinely be deposited (Macleod, 2001; Heavens and Smith, 1957; Hass, 1952). Intermediate refractive indices are accessible by the synthesis of mixed oxides. Nanocomposite mixed oxides can be modeled in the framework of effective medium theories, such as the Bruggeman or the Ping Sheng theory (Bruggeman, 1935; Sheng, 1980), leading to analytical expressions for the resulting optical properties. With all coating processes, care has to be taken to obtain a superior film homogeneity, which is essential for interference filters. Vacuum processes in general yield high quality films, but a considerable investment into vacuum coating machines is necessary already in the start-up phase. The scale-up of a vacuum process, which has been developed in the laboratory, has been demonstrated in many cases (see e.g. Milde et al., 2000). Among the crucial factors regarding the upscaling are the mean-free path of the particles, which does not scale automatically with the machine dimensions, the necessity of a high deposition rate for amortization of the rather expensive equipment, the introduction of a moving substrate inducing gradients within the films, and the coating of the walls, which eventually introduces drifts in the plasma potential. In sol–gel dip coating, the same process parameters as those used in production can be tested on a small scale in the laboratory. The fact that the substrate, the coating machine and the volume of the solution are smaller will not necessarily imply changes of the chemical composition of the solution and the withdrawal speeds. The problems faced here relate to the controlled and clean environment necessary to avoid dust, and the ageing of the solutions with time. Costs rise with the repeated baking of multilayered coatings on large glass panes. One promising option could be special precursors, which

enable film hardening by ultraviolet light (Mennig et al., 1999).

Long-term stability of the proposed coatings is essential for their application and will be the subject of future studies. Coatings need to be humidity resistant and stable at high temperatures and temperature gradients. However, we have reasons to be optimistic: the thin films and the glass substrates used are non-metallic materials and thus less subjected to wet corrosion than e.g. metallic absorber sheets or cermet absorber coatings. Additionally, the differences in thermal dilatation are expected to be smaller than those of cermet coatings on metal sheets. Fully oxidized thin films, which are not susceptible to further oxidation, can be employed. Finally, the multilayered coating can also be on the inner side of the collector glazing where it is not exposed to ambient conditions.

## 5. Conclusions

The general potential of colored thermal solar collectors is promising, and can be expressed by a figure of merit $M$. The principal upper limit for this number $M$ amounts to approximately the value six, which indicates a potential of low energy costs per perceived brightness. The ideal reflectance spectrum of an isolated, sharp peak can be approximated by quarterwave stacks of numerous individual layers. By scaling film thicknesses, the peak position and thus the color of reflection can easily be tuned. Even with a realistic number of individual layers (e.g. five), reasonable performance can be obtained. The difference in refractive indices between the high index and the low index material governs the peak height. The illustrated examples, and the resulting characteristic figures, such as color coordinates, the visible reflectance, the solar transmission, or the figure of merit $M$, encourage putting the idea into practice.

## Acknowledgments

Financial support of this work has been provided by the Swiss Federal Office of Energy SFOE. The authors are grateful to Dr. I. Hagemann and Dr. P.W. Oliveira for inspiring discussions.

## References

Anders, H., 1965. Dünne Schichten Für Die Optik. Wissenschaftliche Verlagsgesellschaft, Stuttgart (English translation 1967. Thin Films in Optics, Focal Press).

ASTM (The American Society for Testing and Materials), 2004. Standard Spectra ASTM E-891, E892, G-159, G-173. Downloadable in electronic form from <http://rredc.nrel.gov/solar/standards/>.

Bergmann, L., Schaefer, C., 1999. Optics of Waves and Particles. Walter de Gruyter, Berlin, New York, p. 452.

Born, M., Wolf, E., 1999. Principles of Optics, seventh ed. Cambridge University Press.

Bruggeman, D.A.G., 1935. Berechnung verschiedener physikalischer Konstanten von heterogenen Substanzen. Ann. Phys. 5. Folge. 24, 636.

CIE International Commission on Illumination, 1986. Colorimetry. CIE Publication 15.2., second ed. Vienna, ISBN 3-900-734-00-3.

Crnjak Orel, Z., Gunde, M.K., 2001. Spectrally selective paint coatings: preparation and characterization. Sol–gel coatings. Sol. Energy Mater. Sol. Cells 68, 337.

Crnjak Orel, Z., Jerman, R., Hodošcek, M., Orel, B., 1990. Characterization of TSSS paint coatings for solar collectors by FTIR spectroscopy. Sol. Energy Mater. 20, 435.

Graf, W., Brucker, F., Köhl, M., Troscher, T., Wittwer, V., Herlitze, L., 1997. Development of large area sputtered solar absorber coatings. J. Non-Cryst. Solids 218, 380.

Hagemann, I.B., 2002. Architektonische Integration der Photovoltaik in die Gebäudehülle. PhD thesis accepted at the Technical University of Aachen, Müller, Köln, ISBN 3-481-01776-6.

Hass, G., 1952. Preparation, properties and optical applications of thin films of titanium dioxide. Vacuum 2, 331.

Heavens, O.S., 1955. Optical Properties of Thin Solid Films. Butterworths, London.

Heavens, O.S., Smith, S.D., 1957. Dielectric thin films. J. Opt. Soc. Am. 47, 469.

Hestnes, A.G., 1999. Building integration of solar energy systems. Sol. Energy 67, 181.

Holland, L., 1956. Vacuum Deposition of Thin Films. Chapman and Hall, London.

Hulstrom, R., Bird, R., Riordan, C., 1985. Spectral solar irradiance data sets for selected terrestrial conditions (solar cell applications). Sol. Cells 15, 365.

Kaluza, L., Orel, B., Drazic, G., Köhl, M., 2001. Sol–gel derived $CuCoMnO_x$ spinel coatings for solar absorbers: Structural and optical properties. Sol. Energy Mater. Sol. Cells 70, 187.

Knittl, Z., 1976. Optics of Thin Films. Wiley, London.

Lazarov, M., Raths, P., Metzger, H., Spirkl, W., 1995. Optical constants and film density of $TiN_xO_y$ solar selective absorbers. J. Appl. Phys. 77, 2133.

Macleod, H.A., 2001. Thin-film Optical Filters. Institute of Physics Publishing, Bristol and Philadelphia.

Mennig, M., Oliveira, P.W., Schmidt, H., 1999. Interference coatings on glass based on photopolymerizable nanomer material. High-performance coatings for transparent systems in large-area and/or high-volume applications. Thin Solid Films 351, 99.

Milde, F., Dimer, M., Hecht, C., Schulze, D., Gantenbein, P., 2000. Large-area production of solar absorbent multilayers by MF-pulsed plasma technology. Vacuum 59, 825.

Niklasson, G.A., Granqvist, C.G., 1983. Surfaces for selective absorption of solar energy: an annotated bibliography 1955–1981. J. Mater. Sci. 18, 3475.

Orel, B., Radoczy, I., Crnjak Orel, Z., 1986. Organic soot pigmented paint for solar panels: formulation, optical properties and industrial application. Sol. Wind Technol. 3, 45.

Orel, B., Vilcnik, A., Šurca Vuk, A., Jelen, B., Köhl, M., Brucker, F., 2003. Thickness insensitive spectrally selective (TISS) paint coatings for glazed and unglazed solar building facades. In: Proceedings of the ISES World Congress, Göteborg, O2 45.

Roecker, C., Affolter, P., Bonvin, J., Gay, J.-B., Müller, A.N., 1995. PV building elements. Sol. Energy Mater. Sol. Cells 36, 381.

Scartezzini, J.-L., Courret, G., 2002. Anidolic daylighting systems. Daylighting Sol. Energy 73, 123.

Schüler, A., Geng, J., Oelhafen, P., Brunold, S., Gantenbein, P., Frei, U., 2000. Application of titanium containing amorphous hydrogenated carbon films (a-C:H/Ti) as optical selective solar absorber coatings. Sol. Energy Mater. Sol. Cells 60, 295.

Schüler, A., Videnovic, I.R., Oelhafen, P., Brunold, S., 2001. Titanium-containing amorphous hydrogenated silicon carbon films (a-Si:C:H/Ti) for durable solar absorber coatings. Sol. Energy Mater. Sol. Cells 69, 271.

Schüler, A., Roecker, C., Scartezzini, J.-L., Boudaden, J., Videnovic, I.R., Ho, R.S.-C., Oelhafen, P., 2004. On the feasibility of colored glazed thermal solar collectors based on thin film interference filters. Sol. Energy Mater. Sol. Cells 84, 241.

Sheng, P., 1980. Theory for the dielectric function of granular composite media. Phys. Rev. Lett. 45, 60.

Stadler, I., 2001. Facade integrated solar thermal collectors. In: Proceedings of the Congress Solar Space Heating, Graz, Austria.

Tabor, H., 1955. US Patent 2,917,817.

Tripanagnostopoulos, Y., Souliotis, M., Nousia, T., 2000. Solar collectors with colored absorbers. Sol. Energy 68, 343.

Weiss, W., Stadler, I., 2001. Facade integration—a new and promising opportunity for thermal solar collectors. In: Proceedings of the Industry Workshop of the IEA Solar Heating and Cooling Programme, Task 26 in Delft, The Netherlands, April 2, 2001. Available from: <http://www.fys.uio.no/kjerne/task26/pdf/industry_workshop_delft.pdf>.